J. Fluid Mech. (1994), *vol.* 260, *pp.* 81–94

The interaction between the mean flow and coherent structures in turbulent mixing layers

By J. COHEN,[1] B. MARASLI[2] AND V. LEVINSKI[1]

[1] Faculty of Aerospace Engineering, Technion – Israel Institute of Technology, Haifa 32000, Israel

[2] Department of Mechanical Engineering, University of Maryland, College Park, MD 20742, USA

(Received 6 December 1991 and in revised form 16 July 1993)

The nonlinear interaction between the mean flow and a coherent disturbance in a two-dimensional turbulent mixing layer is addressed. Based on considerations from stability theory, previous experimental results, in particular the modification of the mean velocity profile, the peculiar growth of the forced shear-layer thickness and the spatial growth of the disturbance amplitude, are explained. A model that assumes a quasi-parallel mean flow having a self-similar mean velocity profile is developed. The model is capable of predicting the downstream evolution of turbulent mixing layers subjected to external excitations.

1. Introduction

Active external excitation of a shear layer at moderately high Reynolds numbers has a profound effect on the evolution of the mean flow as well as on the accompanying turbulent structure, as was shown by Oster & Wygnanski (1982), Ho & Huang (1982), Fiedler & Mensing (1985) and Roberts (1985) for the two-dimensional mixing layer; by Strange & Crighton (1983) and Cohen & Wygnanski (1987*a*, *b*) for the axisymmetric jet; and by Marasli, Champagne & Wygnanski (1991, 1992) for the turbulent wake.

When a turbulent mixing layer is subjected to a two-dimensional periodic disturbance and the frequency of the excitation is an order of magnitude lower than the frequency corresponding to the most amplified waves near the trailing edge of the splitter plate, three distinct regions can be observed (Oster & Wygnanski 1982; Weisbrot & Wygnanski 1988). In the first region (region I), the initial rate of spread of the mixing layer nearly doubled in many instances, until the Strouhal number based on the excitation frequency and on a representative local width of the layer indicated that the mean flow became neutrally stable to the eternal excitation. By neutrally stable we mean a flow in which disturbances are neither amplified nor attenuated. In region I a typical Reynolds stress distribution is positive (Weisbrot & Wygnanski 1988).

In the second region (region II), which extends over a distance corresponding approximately to one wavelength at the excitation frequency, the width of the shear layer decreases slightly whereas the concomitant Reynolds stresses reverse their sign. This suggests that the amplification or decay of the periodic disturbance leads to the divergence or contraction of the mean flow, respectively. In both regions the coherent velocity fluctuations are much more intense than the incoherent ones, thus the total Reynolds stresses (the sum of the coherent and incoherent ones) are mostly due to the coherent wavy disturbance.

In region III the shear layer resumes its linear growth but at a much lower rate. Only in this region are there significant differences between the coherent and total Reynolds

stresses; in fact the two are of opposite sign. The Reynolds stresses associated with the coherent disturbance decay, whereas the incoherent turbulent stresses grow, extracting energy from the mean flow to feed the spreading of the mixing layer. Throughout the development of the shear layer the turbulent Reynolds stress is always positive, meaning that, on average, the direction of energy transfer is *from* the mean *to* the incoherent fluctuations. Similar behaviour in the two-dimensional wake is discussed by Marasli *et al.* (1992).

The divergence of the mean flow is partially responsible for reducing the exponential amplification of a disturbance with increasing downstream distance. The linear theory applied to the slightly diverging mean flow (Bouthier 1972; Crighton & Gaster 1976; Gaster, Kit & Wygnanski 1985) assumes that the mean flow is prescribed and is decoupled from the Reynolds stresses generated by the excitation. Two small scales are necessary to theoretically explain this; the first represents the amplitude of the disturbance, while the second represents the divergence of the mean flow. However, once a discrete periodic perturbation is superposed on the mean flow, these two scales are coupled and the nonlinear terms must be included. In fact, ignoring these terms results in an uncertainty related to the mean flow used in conjunction with this theory, i.e. should one use the unperturbed mean flow or the perturbed one?

Although a lot of theoretical work has been done on the spatial and temporal evolution of a finite-amplitude wave in a turbulent mixing layer, a quantitative comparison between theoretical and experimental results is still lacking. Most of the previous theoretical work was concerned with the flow development in the vicinity of the neutral point, i.e. the point of marginal stability where the disturbance is neither amplified nor decayed. Consequently, in order to 'smooth out' the singularity arising at the critical layer, nonlinear and viscous effects are introduced and the method of matched asymptotic expansions is employed. The introduction of viscosity in the critical layer invalidates the parallel mean flow assumption; therefore, Huerre (1980) and Huerre & Scott (1980) introduced an artificial body force in order to keep the mean flow parallel, while Goldstein & Leib (1988) and Goldstein & Hultgren (1988) introduced a long viscous scale and matched the linear (weakly non-parallel) instability wave solution with the solution obtained in the nonlinear region. Hultgren (1992) recently extended the results of Goldstein & Hultgren to general shear-layer mean velocity profiles and obtained good agreement with *transitional* shear-layer experimental data.

The objective of the present investigation is to demonstrate that the nonlinear coupling between the excited instability wave and the turbulent mean flow is the main cause of shear-layer divergence, and that the nonlinear effects are not confined to a region of finite streamwise extent around the point of marginal stability, but are relevant well upstream of the neutral-point region where the instability wave is still being *linearly* amplified. An *ad hoc* method that assumes a quasi-parallel mean flow having a self-similar velocity profile, describing the spatial interactions between an excited, monochromatic wavy disturbance and the mean flow of a turbulent mixing layer upstream of the neutral point, is proposed in §2. The model calculations are compared with experimental results in §3.

2. Theoretical considerations

The proposed model is aimed at explaining the spatial interaction between an excited, monochromatic wavy disturbance and the mean flow of a turbulent mixing layer, upstream of the neutral point. It is assumed that in the linear regime where the

wave is amplified, the viscosity has virtually no effect and consequently the viscous terms are neglected. The disturbance growth rates, although small, are sufficiently high (compared to other shear flows such as wakes) for the artificial wave train to dominate the flow. Consequently, as was discussed in §1, the Reynolds stresses are almost entirely due to the coherent disturbance.

In the present analysis a direct account of the complex interaction between the incoherent fluctuations and the mean flow is not attempted. Instead, based on the experimental observations mentioned above, the following algorithm is proposed. The downstream distance is divided into small equal intervals. The length of each interval is chosen to be much smaller than a characteristic lengthscale representing the divergence of the mean flow. At each interval the spreading of the mean flow is attributed only to the coherent Reynolds stress. The stability equations for each one of the intervals are derived and solved. From the solutions of these equations the local streamwise derivatives of the mean velocity and the amplitude of the wave are obtained. Only the local change of the momentum thickness is used to construct the new mean flow at the advanced streamwise interval. The detailed change in shape of the mean velocity profile over a long streamwise distance is not considered here since it depends on the accumulated effect of the incoherent Reynolds stress. This effect, however, is partially accounted for by using a self-similar mean velocity profile, in accordance with previous experimental data (Oster & Wygnanski 1982; Gaster *et al.* 1985).

2.1. *Governing equations*

The non-dimensional equation of motion describing the two-dimensional inviscid and incompressible mixing layer in Cartesian coordinates is given by

$$\left\{\frac{\partial}{\partial t}+\frac{\partial \Psi}{\partial y}\frac{\partial}{\partial x}-\frac{\partial \Psi}{\partial x}\frac{\partial}{\partial y}\right\}\nabla^2\Psi = 0, \tag{1}$$

where the stream function $\Psi(x, y, t)$ satisfies the relations

$$U = \frac{\partial \Psi}{\partial y} \quad \text{and} \quad V = -\frac{\partial \Psi}{\partial x}. \tag{2}$$

Here U and V represent the streamwise and transverse components of the velocity vector, respectively, x is the streamwise coordinate and y is the transverse coordinate. Since the relevant scales are the local integral scale, θ, of the shear layer and the positive velocity difference between the upper and lower streams of the mixing layer, U_2-U_1, these quantities were used to render all variables dimensionless, i.e.

$$U = \frac{\hat{U}}{U_2-U_1}, \quad V = \frac{\hat{V}}{U_2-U_1}, \quad x = \frac{\hat{x}}{\theta}, \quad y = \frac{\hat{y}-Y_{\frac{1}{2}}}{\theta}, \quad \Psi = \frac{\hat{\Psi}}{\theta(U_2-U_1)}. \tag{3}$$

All dimensional variables are denoted by the hat symbol while time-averaged (mean) quantities are denoted by the overbar. The integral lengthscale θ, which is often referred to as the momentum thickness, is given by

$$\theta = \int_{-\infty}^{+\infty} \frac{\hat{U}-U_1}{U_2-U_1}\left(1-\frac{\hat{U}-U_1}{U_2-U_1}\right)\mathrm{d}\hat{y}, \tag{4}$$

and $Y_{\frac{1}{2}}$ is the value of $\hat{y}$ where the mean velocity equals the convective velocity $U_c \equiv \frac{1}{2}(U_1+U_2)$.

Assuming that the mean flow is perturbed by a disturbance of $O(\epsilon)$ ($\epsilon \ll 1$), one may attempt to find a power-series solution to the stream function satisfying (1). Around an arbitrary streamwise position x_0, the mean flow is assumed to be quasi-parallel and the power-series expansion is given by

$$\Psi(x,y,t) = \Psi_0(y) + \epsilon\Psi_1(x,y,t) + \epsilon^2\Psi_2(x,y,t) + \ldots, \tag{5}$$

where $\Psi_0(y) = \bar{\Psi}(x_0, y)$. Since to leading order the mean flow is assumed to be parallel, the coefficients in the linearized set of equations at $O(\epsilon)$ depend only on y and the equations admit solutions which depend on x and t exponentially. Therefore, solutions of the form

$$\Psi_1 = \Phi_1(y)\,\mathrm{e}^{\mathrm{i}(\alpha x - \beta t)} + \Phi_1^*(y)\,\mathrm{e}^{-\mathrm{i}(\alpha^* x - \beta t)} \equiv \psi_1 + \psi_1^*, \tag{6}$$

which represent two-dimensional travelling waves, are considered. Here the asterisk denotes complex conjugation and α is a complex eigenvalue ($\alpha = \alpha_r + \mathrm{i}\alpha_i$), of which the real part is the non-dimensional wavenumber while the imaginary part represents the rate of amplification. The non-dimensional frequency β is real since the analysis is limited to *spatially* amplifying waves.

Substitution of (5) into (1) yields to $O(\epsilon)$

$$\left\{\left(\frac{\partial}{\partial t} + U_0\frac{\partial}{\partial x}\right)\left(\frac{\partial^2}{\partial x^2} + \frac{\partial^2}{\partial y^2}\right) - U_0''\frac{\partial}{\partial x}\right\}\Psi_1 \equiv \mathscr{L}\{\Psi_1\} = 0, \tag{7}$$

where $U_0 = \mathrm{d}\Psi_0/\mathrm{d}y$ and $U_0'' = \mathrm{d}^3\Psi_0/\mathrm{d}y^3$. Here prime denotes differentiation with respect to y. Further, by substituting (6) into (7) one obtains the well-known Rayleigh equation,

$$\left\{(U_0 - c)\left(\frac{\mathrm{d}^2}{\mathrm{d}y^2} - \alpha^2\right) - U_0''\right\}\Phi_1 = 0, \tag{8}$$

where $c = \beta/\alpha$.

Selecting terms of $O(\epsilon^2)$ yields

$$\mathscr{L}\{\Psi_2\} = -\left(\frac{\partial\Psi_1}{\partial y}\frac{\partial}{\partial x} - \frac{\partial\Psi_1}{\partial x}\frac{\partial}{\partial y}\right)\left(\frac{\partial^2\Psi_1}{\partial x^2} + \frac{\partial^2\Psi_1}{\partial y^2}\right) \equiv -RS, \tag{9}$$

where

$$RS = RSH + RSM. \tag{10}$$

The linear operator $\mathscr{L}$ is defined in (7) and $-RS$ represents the interaction of a wave with itself. Such an interaction results in the generation of the second harmonic via the term ψ_1^2 which is denoted by *RSH*, and a contribution to the mean flow via the cross-product $\psi_1\psi_1^*$, denoted by *RSM*.

As shown in Appendix A, *RSM* can be cast in the form

$$RSM = -2\alpha_i\,\mathrm{e}^{-2\alpha_i x}\left\{\frac{\partial F}{\partial y} + 4\alpha_i^2\tau\right\}, \tag{11}$$

where

$$F \equiv |\Phi_1'|^2 - |\alpha\Phi_1|^2 - \frac{U_0 U_0''|\Phi_1|^2}{|U_0 - c|^2}, \tag{12}$$

and

$$\tau \equiv \frac{\mathrm{i}}{2\alpha_i}(\alpha^*\Phi_1^*\Phi_1' - \alpha\Phi_1\Phi_1^{*\prime}). \tag{13}$$

For future reference note that τ, which represents the ratio between the coherent shear stress and the growth rate of the wavy disturbance, is of $O(1)$, even in the limit $|\alpha_i| \to 0$ (see Appendix B).

2.2. *The streamwise variation of the local mean flow*

From (5) and (6) it follows that the mean flow $\bar{\Psi}(x,y)$, consists of a parallel flow $\Psi_0(y)$ and a small modification $\epsilon^2\bar{\Psi}_2(x,y)$ (the mean part of $\epsilon^2\Psi_2(x,y,t)$), induced by the unsteady periodic perturbation. Since (9) is linear, in order to determine $\bar{\Psi}_2(x,y)$ we solve the equation including only the mean part of the right-hand side, *RSM*, i.e.

$$\mathscr{L}\{\bar{\Psi}_2\} = 2\alpha_i \mathrm{e}^{-2\alpha_i x}\left\{\frac{\partial F}{\partial y} + 4\alpha_i^2 \tau\right\}. \tag{14}$$

The solution $\bar{\Psi}_2$ can be decomposed into

$$\bar{\Psi}_2 = \Psi_{hom} + \Psi_m, \tag{15}$$

where Ψ_{hom} and Ψ_m are the homogeneous and particular solutions of (14), respectively. From the right-hand side of (14), it is evident that $\bar{\Psi}_2$ depends on y and the streamwise lengthscale

$$x_1 \equiv |\alpha_i| x, \tag{16}$$

and has the form

$$\bar{\Psi}_2 = \Psi_{hom}(x_1, y) + \mathrm{e}^{-2\alpha_i x}\Phi_m(y), \tag{17}$$

together with the boundary condition

$$\frac{\partial}{\partial x_1}\bar{\Psi}_2(x_1 \to -\infty, y) = 0. \tag{18}$$

Substituting (17) into (14) and keeping only those terms at most linear in α_i, we obtain

$$\frac{\partial}{\partial x_1}(U_0 \Psi''_{hom}(x_1,y) - U_0'' \Psi_{hom}(x_1,y)) = 0, \tag{19}$$

and

$$U_0 \Phi_m'' - U_0'' \Phi_m = -\frac{\partial F}{\partial y}. \tag{20}$$

The streamwise-dependent solution of (19) and the solution of (20) are determined by the method of variation of parameters. Thus

$$\Psi_{hom} = g_1(x_1)\, U_0 + g_2(x_1)\, U_0 \int_0^y \frac{\mathrm{d}\check{y}}{U_0^2(\check{y})}, \tag{21}$$

with

$$\frac{\mathrm{d}}{\mathrm{d}x_1} g_1(x_1 \to -\infty) = \frac{\mathrm{d}}{\mathrm{d}x_1} g_2(x_1 \to -\infty) = 0, \tag{22}$$

and

$$\Psi_m = \mathrm{e}^{-2\alpha_i x}\Phi_m(y) = \mathrm{e}^{-2\alpha_i x}\left\{D_1\, U_0(y) + U_0(y)\, G(y) + D_2\, U_0(y) \int_0^y \frac{\mathrm{d}\check{y}}{U_0^2(\check{y})}\right\}, \tag{23}$$

where

$$G(y) = -\int_0^y \frac{F(\check{y})}{U_0^2(\check{y})}\mathrm{d}\check{y}. \tag{24}$$

In order to evaluate the unknown constants D_1 and D_2, and the unknown functions $g_1(x_1)$ and $g_2(x_1)$, we follow the matching procedure used by Goldstein & Leib (1988). Thus, we shall match the outer expansion of the inner mixing layer solution $\bar{\Psi}_2$ with the inner expansion of the outer potential flow solution $\bar{\Psi}_P$.

On one hand, away from the mixing layer ($y \gg 1$), the potential flow is a function

of two long scales, $x_1 = |\alpha_i| x$ and $y_1 = |\alpha_i| y$, and its asymptotic expansion for $y_1 \ll 1$ is given by

$$\bar{\Psi}_P(x_1, y_1) = \bar{\Psi}_P^{\pm}(x_1, 0) + \frac{\partial \bar{\Psi}_P^{\pm}}{\partial y_1}(x_1, 0)\, y_1 + O(\alpha_i^2), \tag{25}$$

where the subscripts + and − refer respectively, to the regions $y > 0$ and $y < 0$. Consequently the asymptotic forms of the potential velocities are given by

$$\bar{u}_P^{\pm}(x_1, 0) = |\alpha_i| \frac{\partial \bar{\Psi}_P^{\pm}}{\partial y_1}(x_1, 0) + O(\alpha_i^2), \tag{26}$$

and

$$\bar{v}_P^{\pm}(x_1, 0) = -|\alpha_i| \frac{\partial \bar{\Psi}_P^{\pm}}{\partial x_1}(x_1, 0) + O(\alpha_i^2). \tag{27}$$

On the other hand, the streamwise-dependent asymptotic mixing layer solution for the streamwise velocity as $y \to \pm\infty$ is given by

$$\bar{u}_2^{\pm}(x_1, \pm\infty) = \frac{\partial \bar{\Psi}_2^{\pm}}{\partial y}(x_1, \pm\infty) = \frac{g_2(x_1)}{U_0^{\pm}} + \frac{D_2}{U_0^{\pm}} e^{-2\alpha_i x} + O(\alpha_i^2), \tag{28}$$

which can also be written as

$$U_0^{+} \frac{d\bar{u}_2^{+}}{dx_1} = U_0^{-} \frac{d\bar{u}_2^{-}}{dx_1} + O(\alpha_i^2). \tag{29}$$

It should be noted that the same relation can be obtained directly by integrating the mean part of (9) across the mixing layer.

Comparison of (26) with (28) shows that

$$g_2(x_1), D_2 \sim O(|\alpha_i\, \bar{\Psi}_P^{\pm}(x_1, 0)|). \tag{30}$$

Similarly, the asymptotic expansion of the vertical velocity $\bar{v}_2$ is given by

$$\bar{v}_2^{\pm}(x_1, \pm\infty) = -|\alpha_i| \frac{dg_1}{dx_1} U_0^{\pm} + 2\alpha_i e^{-2\alpha_i x} \{D_1 U_0^{\pm} + U_0^{\pm} G^{\pm}\} + O(\alpha_i^2), \tag{31}$$

and matching with (27) shows that

$$g_1(x_1), D_1 \sim O(|\bar{\Psi}_P^{\pm}(x_1, 0)|). \tag{32}$$

Since the streamwise derivatives of $\bar{u}_P$ and $\bar{v}_P$ are harmonic conjugate functions, their boundary values are related by the Hilbert transforms

$$\frac{d\bar{v}_P^{\pm}}{dx_1}(x_1) = \mp \frac{1}{\pi} \int_{-\infty}^{\infty} \frac{d\bar{u}_P^{\pm}(\check{x}_1)}{d\check{x}_1} \frac{d\check{x}_1}{\check{x}_1 - x_1}, \tag{33}$$

where the bar indicates that the Cauchy principal value is to be taken.

Provided that $\bar{u}_P^{\pm}(x_1, 0)$ and $\bar{v}_P^{\pm}(x_1, 0)$ are replaced by the asymptotic expansions of the inner variables $\bar{u}_2^{\pm}$ and $\bar{v}_2^{\pm}$ respectively, one can get the following relation from (33):

$$U_0^{+} \frac{d\bar{v}_2^{+}}{dx_1}(x_1) + U_0^{-} \frac{d\bar{v}_2^{-}}{dx_1}(x_1) = -\frac{1}{\pi} \int_{-\infty}^{\infty} \left(\frac{d\bar{u}_2^{+}}{d\check{x}_1}(\check{x}_1)\, U_0^{+} - \frac{d\bar{u}_2^{-}}{d\check{x}_1}(\check{x}_1)\, U_0^{-} \right) \frac{d\check{x}_1}{\check{x}_1 - x_1}. \tag{34}$$

Substitution of (29) into (34) yields

$$U_0^{+} \frac{d\bar{v}_2^{+}}{dx_1}(x_1) = -U_0^{-} \frac{d\bar{v}_2^{-}}{dx_1}(x_1) + O(\alpha_i^2), \tag{35}$$

and by using (31) one obtains

$$\frac{\mathrm{d}^2 g_1}{\mathrm{d}x_1^2}(x_1) = 0 \tag{36}$$

and

$$U_0^{+^2}[D_1 + G(\infty)] + U_0^{-^2}[D_1 + G(-\infty)] = 0. \tag{37}$$

The boundary conditions (18) and (22) together with (36) imply that

$$\frac{\mathrm{d}g_1}{\mathrm{d}x_1}(x_1) = 0. \tag{38}$$

Using the definition $U_2 = U_0^+$ and $U_1 = U_0^-$, the constant D_1 is determined to be

$$D_1 = -\frac{G(\infty)\, U_2^2 + G(-\infty)\, U_1^2}{U_2^2 + U_1^2}. \tag{39}$$

Substituting (21) and (23) into the streamwise derivative of (17), and using (30), (32) and (38), the streamwise variation of the local mean velocity is obtained as

$$\frac{\partial}{\partial x}\left(\frac{\partial \bar{\Psi}_2}{\partial y}\right) = -2\alpha_i \mathrm{e}^{-2\alpha_i x}\, \Phi_m'(y) = -2\alpha_i \mathrm{e}^{-2\alpha_i x}\left(U_0'(y)\,(G(y) + D_1) + \frac{F(y)}{U_0(y)}\right) + O(\alpha_i^2). \tag{40}$$

2.3. *The spatial development of the mean flow and the disturbances*

From (5) and (40) it follows that the streamwise variation of the mean flow is of $O(|\epsilon^2 \alpha_i|)$. Therefore, for any streamwise interval $\Delta x \ll 1/|\epsilon^2 \alpha_i|$, the functions U_0, Φ_1, Φ_m and their derivatives are assumed to depend only on the y-coordinate, while the eigenvalues α and c are assumed to be constant.

For the numerical computation the downstream distance is divided into small equal increments denoted by x_j, $j = 0, 1, 2, \ldots$. The disturbance at a given streamwise location within the interval $\{x_j, x_{j+1}\}$ has the form

$$\epsilon \Psi_1(x, y, t) = A(x)\, \Phi_1(x_j, y)\, \mathrm{e}^{\mathrm{i}\Theta(x,t)} + A^*(x)\, \Phi_1^*(x_j, y)\, \mathrm{e}^{-\mathrm{i}\Theta(x,t)}, \tag{41}$$

where the amplitude and phase are given by $A(x) = A(x_j)\exp[-\alpha_i(x - x_j)]$ and $\Theta(x, t) = \Theta(x_j, t) + \alpha_r(x - x_j)$, respectively.

In the present analysis the mean velocity profile is assumed to be self-similar, with the x-axis ($y = 0$) defining the position at which the mean velocity has the value U_c. Within any given interval $\{x_j, x_{j+1}\}$, U_0 is taken to be independent of x and its profile in the y-direction is a function only of $y/\theta(x_j)$. Therefore, in order to advance to the next downstream location x_{j+1}, the streamwise variation of the momentum thickness has to be calculated. Using the expression for the streamwise variation of the mean velocity (40) and the definition (4), the change in θ is given by

$$\theta(x_{j+1}) - \theta(x_j) = -2\alpha_i\, A(x_j)\, A^*(x_j)\, \Delta x \int_{-\infty}^{\infty} \Phi_m'(x_j, y)\left[1 - 2\left(U_0(x_j, y) - \frac{U_1}{U_2 - U_1}\right)\right] \mathrm{d}y, \tag{42}$$

where $\Delta x = x_{j+1} - x_j$ and $U_0(x_j, y)$ is the self-similar velocity profile at x_j. The amplitude and phase of the wave at the advanced streamwise location are given by

$$A(x_{j+1}) = A(x_j) + \frac{\mathrm{d}A(x_j)}{\mathrm{d}x}\Delta x = A(x_j)(1 - \alpha_i \Delta x), \tag{43}$$

and $$\Theta(x_{j+1}, t) = \Theta(x_j, t) + \alpha_r(x_j)\Delta x. \tag{44}$$

For a given initial value of the momentum thickness, the self-similar mean velocity profile is determined, and the linearized equation (8) for the periodic disturbance is solved. Then, for a given initial disturbance amplitude, the streamwise variation of the mean velocity is obtained from (40), whereby the momentum thickness at the advanced streamwise position is calculated from (42). The disturbance amplitude at the next downstream position is calculated using (43). This procedure is repeated at each one of the streamwise positions, until the neutral point is reached.

3. Comparison with experimental data

3.1. *The local modification of the mean velocity profile*

In this section, the theoretical computations are compared to experimental data, which were obtained at the two-dimensional mixing-layer facility at Tel-Aviv University with the extensive cooperation of I. Weisbrot. For the details of the facility and experimental procedures the reader is referred to Oster & Wygnanski (1982) and Weisbrot & Wygnanski (1988). The higher-stream velocity, U_2, was kept at 10 m s^{-1} while the lower-stream velocity, U_1, was varied to produce two velocity ratios of $R = U_1/U_2 = 0.2$ and 0.6. At a given downstream position, two mean velocity profiles were measured: first without any artificial disturbance, and second with the mixing layer subjected to a periodic disturbance having a dimensional frequency F_f. The normalized difference between the two experimental mean profiles represents qualitatively the modification of the streamwise mean velocity $\Phi'_m(y)$ (see (40)), induced by the unsteady excited wave.

Two sets of data, which were obtained at two different downstream locations corresponding to a single local Strouhal number $(F_f\theta/(U_1+U_2))$ of 0.02 and to $R = 0.2$, are presented in figure 1(*a*) together with their respective unforced mean velocity profiles. The frequencies of the excited disturbances in the two locations were 60 and 42 Hz while the corresponding momentum thicknesses were 4.01 and 5.72 mm. The fact that both sets follow the same curve demonstrates that the local Strouhal number is the single important parameter for a given velocity ratio. The modification of the mean profile is asymmetric, with the lower-velocity side broader than the higher-velocity side.

Similar experimental results for $R = 0.6$ and two different values of the Strouhal number are shown in figure 1(*b*, *c*). In contrast to the $R = 0.2$ data, the modification of the mean flow is close to an antisymmetric shape, modifying the higher- and lower-velocity sides of the mixing layer by nearly equal amounts.

The theoretical modification of the mean flow, computed from (40), is presented in figure 1(*d*–*f*), corresponding to the experimental result presented in figure 1(*a*–*c*), respectively. The mean velocity profile used in the calculations (see Gaster *et al.* 1985) is given by

$$U_0(\eta) - \frac{U_1}{U_2 - U_1} = 0.5[1 + (1 + C_1 \operatorname{sech}^2(\eta)) \tanh(\eta)], \tag{45}$$

where $\eta = C_2 y$. The constant C_2 is related to C_1 by the definition of the quasi-two-dimensional momentum thickness and is given by

$$C_2 = \tfrac{1}{2} - \tfrac{1}{3}C_1 - \tfrac{1}{15}C_1^2. \tag{46}$$

In the calculations that follow, C_1 is chosen to be either 0 or 0.67, corresponding to the classical 'tanh' profile and the improved profile suggested by Gaster *et al.* (1985),

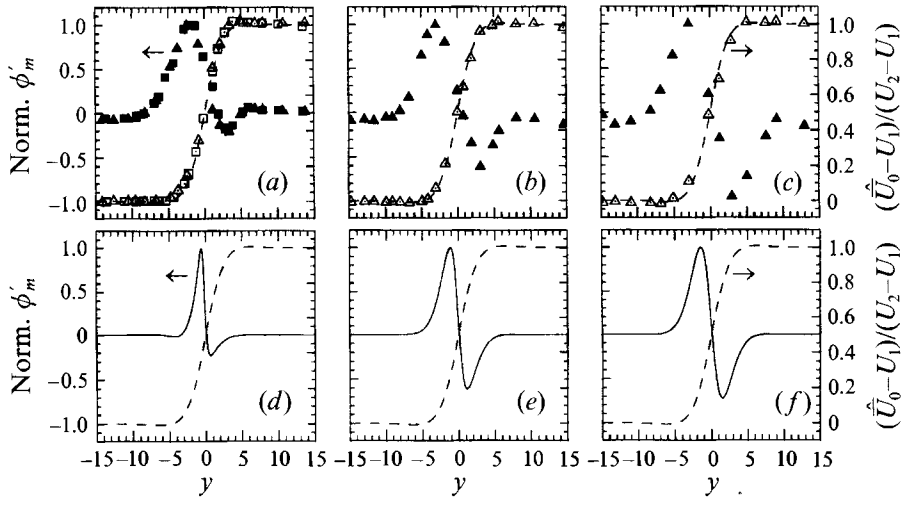

FIGURE 1. Experimental normalized mean velocity profiles (open symbols), corresponding wave-induced mean profile modifications (filled symbols) and comparison with theory: (*a*) $U_1 = 2$ m s^{-1}, $U_2 = 10$ m s^{-1}, $St_\theta = 0.02$; △, $F_f = 60$ Hz, $\hat{x} = 150$ cm, $\theta = 4.01$ mm; ⊡, $F_f = 42$ Hz, $\hat{x} = 200$ cm, $\theta = 5.71$ mm; (*b*) $U_1 = 6$ m s^{-1}, $U_2 = 10$ m s^{-1}, $St_\theta = 0.0125$, $F_f = 42$ Hz, $\hat{x} = 300$ cm, $\theta = 4.76$ mm; (*c*) $U_1 = 6$ m s^{-1}, $U_2 = 10$ m s^{-1}, $St_\theta = 0.0077$, $F_f = 42$ Hz, $\hat{x} = 150$ cm, $\theta = 2.92$ mm; (*d*) theoretical counterpart of (*a*); (*e*) theoretical counterpart of (*b*); (*f*) theoretical counterpart of (*c*).

respectively. For the results presented in figure 1 the analytical expressions, given by (45) with $C_1 = 0.67$, was used to represent the unforced mean profile in the computation; the corresponding computational results for $C_1 = 0$ are similar.

For all three data sets the qualitative agreement between the measurements and the theory is good. In particular, the broadening of the higher-velocity side of the mixing layer, as the velocity ratio is increased and the Strouhal number is decreased, is well captured by the computations. However, the experimental distributions are substantially broader than the corresponding theoretical predictions. This is partially attributed to the fact that while the experimental modification of the mean flow shown in figure 1 is a result of a cumulative effect integrated over the entire upstream distance, the theoretical modification represents only the local change of the velocity profile. Therefore, at this stage only a qualitative comparison is presented.

3.2. *The spatial development of the mean flow and the disturbances*

The variation of the momentum thickness with downstream distance (obtained by Oster & Wygnanski 1982) is shown in figure 2. The influence of the forcing frequency on the spreading rate of the two-dimensional turbulent shear layer is demonstrated in figure 2(*a*), while the effects of the velocity ratio R are shown in figure 2(*b*). Since for a given velocity ratio $R = U_1/U_2$ the model suggests that the important parameter in the problem is the local Strouhal number (via the linear problem), when these results are scaled properly, all the data points indeed collapse around the dashed curve which represents the theoretical results (figure 2*c*). In these calculations the mean velocity profile was assumed to fit the formula given by (45) with $C_1 = 0$. A similar curve corresponding to $C_1 = 0.67$ is shown by the solid line. The ordinate in figure 2(*c*) is the local Strouhal number and the abscissa is a measure of the downstream distance in terms of wavelengths (shifted by a distance x_0). Marasli *et al.* (1992) obtained similar results in a plane turbulent wake. The inclusion of the velocity ratio in the abscissa is an outcome of the study done by Monkewitz & Huerre (1982) and the numerical

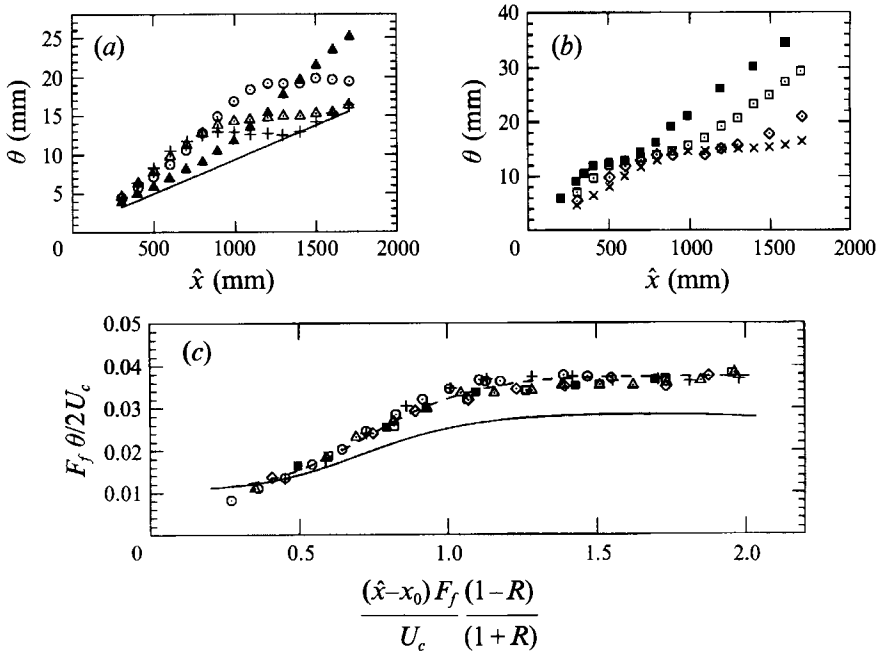

FIGURE 2. Momentum thickness data for forced mixing layers: (*a*) $R = 0.6$; ——, unforced; ▲, $F_f = 30$; ⊙, 40; △, 50; +, 60 Hz; (*b*) $F_f = 50$ Hz; ■, $R = 0.3$; ⊡, 0.4; ◇, 0.5; ×, 0.6; (*c*) non-dimensional data compared with theoretical calculations: ——, $C_1 = 0.67$; – – – –, $C_1 = 0$. Experimental data from Oster & Wygnanski (1982).

simulations of Riley & Metcalfe (1980). During the downstream integration, all dimensional variables were made dimensionless using the initial momentum thickness and the velocity difference across the shear layer as constant reference scales.

As can be seen from figure 2 the theoretical prediction depends on the self-similar profile, in particular the choice of C_1 in (45). An *a priori* choice of the self-similar profile is difficult since it depends on the interaction between the incoherent fluctuations and the instability wave and other factors which are not addressed in this paper. However, if the Strouhal number at the plateau region (region II) is matched to the neutral Strouhal number computed for a particular mean velocity profile and a given excitation frequency, the prediction of the streamwise evolution of the shear-layer thickness is good. The good agreement between the experimental data and the theoretical computation (for $C_1 = 0$) indicates that indeed the coupling between the mean field and the periodic excited disturbance controls the spreading of the shear layer. As long as the amplitude of the perturbations is small, the associated spatial developments are identical up to a translational shift, x_0. In other words, before the nonlinear coupling becomes significant, the distance where the disturbance is amplified with a constant exponent is longer for a disturbance having a lower initial amplitude and vice versa.

The momentum thickness initially grows almost linearly with x and then, when the local Strouhal number exceeds the neutral value, a parallel region (constant θ) is generated. The length of the plateau is determined by the amplitude level of the lower-frequency disturbances relative to the forced wave amplitude.

Next, the predicted development of both the momentum thickness and the disturbance amplitude is compared with the experimental results obtained by Gaster

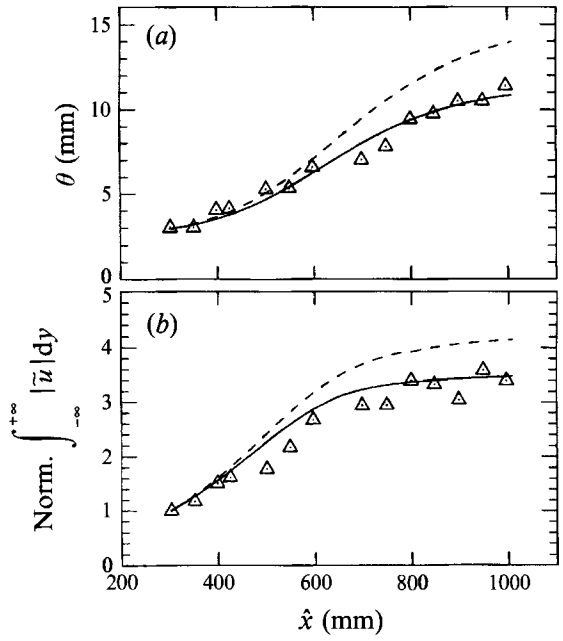

FIGURE 3. (*a*) Streamwise variation of the momentum thickness; (*b*) normalized amplitude of the induced wave. △, data of Gaster *et al.* (1985); ——, theoretical calculation with $C_1 = 0.67$; – – –, with $C_1 = 0$.

et al. (1985). In figure 3(*a*) the streamwise variation of the momentum thickness is shown, while in figure 3(*b*) the corresponding variation of the normalized integral amplitude, $\int_{-\infty}^{\infty} |\tilde{u}|\,\mathrm{d}y$ (the tilde denotes the coherent part), of the excited wave is depicted. The symbols correspond to the experimental data points, while the solid and dashed lines represent the theoretical results, where the disturbance amplitude $|\tilde{u}| = |u_1(x,y)| = 2|A(x)\,\Phi_1'(x,y)|$. The dashed and solid lines correspond to theoretical solutions using the self-similar profile given by (45) with $C_1 = 0$ and 0.67, respectively. The agreement between the experimental results and the theoretical calculation based on the improved self-similar profile ($C_1 = 0.67$) is much better. As was indicated by Gaster *et al.*, this profile provided a better fit to the data than the regular 'tanh' profile. It should be noted that in the present calculations only the initial momentum thickness was known from the experiments. However, since the associated spatial development is identical up to a translational shift (see the discussion with respect to figure 2), the initial amplitude was chosen so that its initial slope of growth best fitted the experimental results.

A similar comparison with the experimental data obtained by Weisbrot & Wygnanski (1988) is shown in figure 4, where the downstream variation of the amplitude of the lateral component of the velocity perturbation, $|\tilde{v}|$, is included as well. Note that only the initial θ and $\tilde{v}$ amplitudes from the theory and the experiments are matched, while $\tilde{u}$ is calculated. The prediction based on the improved self-similar profile underestimates the data for θ and $\tilde{v}$, while the prediction based on the regular 'tanh' profile overestimates the data for θ, $\tilde{u}$ and $\tilde{v}$.

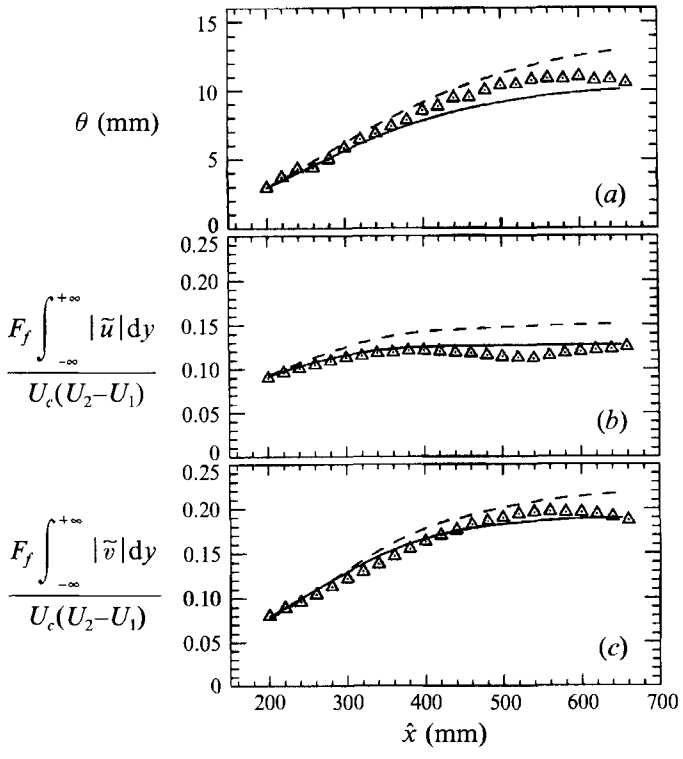

FIGURE 4. Streamwise variation of (*a*) the momentum thickness, and normalized amplitude of the induced wave; (*b*) the streamwise component; (*c*) the cross-stream component. △, data of Weisbrot & Wygnanski (1988); ——, theoretical calculation with $C_1 = 0.67$; – – – –, with $C_1 = 0$.

4. Conclusions

The modification of the mean flow in turbulent mixing layers caused by instability waves is predicted by an inviscid nonlinear spatial theory, provided the amplification rates are small. Furthermore, the spatial evolution of both the disturbance amplitude and the width of the shear layer can be predicted by a simple quasi-parallel model. It is demonstrated that the local Strouhal number, representing the ratio between the shear-layer thickness and the streamwise wavelength of the disturbance, is the important parameter controlling the evolution of the mixing layer for a given initial disturbance amplitude. Since in the initial region where the wave is amplified the coherent Reynolds stresses dominate the flow, the analysis, which assumes a self-similar mean velocity profile, is successful in predicting the downstream evolution of turbulent mixing layers subjected to external excitations.

The authors wish to thank I. Wygnanski for many stimulating discussions and I. Weisbrot for his extensive cooperation in acquiring some of the experimental mixing-layer data.

Appendix A

The right-hand side of (9) in §2.1 is given by

$$RS = \left(u_1 \frac{\partial}{\partial x} + v_1 \frac{\partial}{\partial y}\right)\left(-\frac{\partial v_1}{\partial x} + \frac{\partial u_1}{\partial y}\right). \tag{A 1}$$

The expressions for the streamwise and transverse velocities to order $O(\epsilon)$ are

$$u_1 = \partial \Psi_1/\partial y = \Phi_1' e^{i\Theta} + \Phi_1^{*'} e^{-i\Theta^*}, \tag{A 2}$$

and

$$v_1 = -\partial \Psi_1/\partial x = -i\alpha \Phi_1 e^{i\Theta} + i\alpha^* \Phi_1^* e^{-i\Theta^*}, \tag{A 3}$$

respectively, where

$$\Theta = \alpha x - \beta t. \tag{A 4}$$

Using the continuity equation, (A 1) can be cast in the form

$$RS = -\frac{\partial^2(u_1 v_1)}{\partial x^2} + \frac{\partial^2(u_1 v_1)}{\partial y^2} - \frac{\partial^2(v_1^2)}{\partial x \partial y} + \frac{\partial^2(u_1^2)}{\partial x \partial y}. \tag{A 5}$$

The time-average of (A 5) is given by

$$RSM = -\frac{\partial^2(\overline{u_1 v_1})}{\partial x^2} + \frac{\partial^2(\overline{u_1 v_1})}{\partial y^2} - \frac{\partial^2(\overline{v_1^2})}{\partial x \partial y} + \frac{\partial^2(\overline{u_1^2})}{\partial x \partial y}, \tag{A 6}$$

where the Reynolds stresses are

$$\overline{u_1^2} = 2|\Phi_1'|^2 e^{-2\alpha_i x}, \quad \overline{v_1^2} = 2|\alpha \Phi_1|^2 e^{-2\alpha_i x}, \tag{A 7), (A 8}$$

and

$$\overline{u_1 v_1} = i(\alpha^* \Phi_1' \Phi_1^* - \alpha \Phi_1 \Phi_1^{*'}) e^{-2\alpha_i x} \equiv 2\alpha_i \tau e^{-2\alpha_i x}. \tag{A 9}$$

Thus,

$$RSM = -2\alpha_i e^{-2\alpha_i x} \left\{ 4\alpha_i^2 \tau + \frac{\partial}{\partial y} \left[-\frac{\partial \tau}{\partial y} - 2|\alpha \Phi_1|^2 + 2|\Phi_1'|^2 \right] \right\}. \tag{A 10}$$

Using the Rayleigh equation it can be shown that

$$\frac{\partial \tau}{\partial y} = |\Phi_1'|^2 - |\alpha \Phi_1|^2 + \frac{U_0 U_0'' |\Phi_1|^2}{|U_0 - c|^2}, \tag{A 11}$$

and finally the expression for RSM is given by

$$RSM = -2\alpha_i e^{-2\alpha_i x} \left\{ \frac{\partial}{\partial y} \left[|\Phi_1'|^2 - |\alpha \Phi_1|^2 - \frac{U_0 U_0'' |\Phi_1|^2}{|U_0 - c|^2} \right] + 4\alpha_i^2 \tau \right\}. \tag{A 12}$$

Appendix B

From (A 11) in Appendix A, it is clear that away from the critical layer $2\alpha_i \partial \tau/\partial y \approx O(\alpha_i)$. In the critical layer, the first two terms on the right-hand side of (A 11) are of $O(1)$. Therefore, we concentrate on the last term on the right-hand side of (A 11). Integrating this term across the critical layer we obtain:

$$I = \int_{Y_c - \Delta}^{Y_c + \Delta} \frac{U_0 U_0'' |\Phi_1|^2}{|U_0 - c|^2} \mathrm{d}y, \tag{B 1}$$

where Y_c is the y position at which $U_0 = c_r$, and Δ is a distance much greater than the critical-layer thickness, which is proportional to c_i, such that

$$1 \gg \Delta \gg c_i. \tag{B 2}$$

Then, using the Taylor series expansion around Y_c we obtain

$$I = \frac{\pi U_0(Y_c)\, U_0''(Y_c) |\Phi_1(Y_c)|^2}{c_i\, U_0'(Y_c)} \approx O\left(\left| \frac{U_0''(Y_c)}{c_i} \right| \right). \tag{B 3}$$

For the hyperbolic tangent profile used in the paper it can be shown that

$$U_0''(Y_c) \approx O(c_r - U_0(Y_{\frac{1}{2}})), \tag{B 4}$$

and

$$U_0''(Y_c)/c_i \approx O([c_r - U_0(Y_{\frac{1}{2}})]/c_i) \tag{B 5}$$

which was shown by Robinson (1974) to be of $O(1)$.

REFERENCES

Bouthier, M. 1972 Stabilité linéaire des écoulements presque paralléles. *J. Méc.* **11**, 599.

Cohen, J. & Wygnanski, I. 1987*a* The evolution of instabilities in the axisymmetric jet. Part 1. The linear growth of disturbances near the nozzle. *J. Fluid Mech.* **176**, 191.

Cohen, J. & Wygnanski, I. 1987*b* The evolution of instabilities in the axisymmetric jet. Part 2. The flow resulting from the interaction between two waves. *J. Fluid Mech.* **176**, 221.

Crighton, D. G. & Gaster, M. 1976 Stability of slowly diverging jet flow. *J. Fluid Mech.* **77**, 397.

Fiedler, H. E. & Mensing, P. 1985 The plane turbulent shear layer with periodic excitation. *J. Fluid Mech.* **150**, 281.

Gaster, M., Kit, E. & Wygnanski, I. 1985 Large-scale structures in a forced turbulent mixing layer. *J. Fluid Mech.* **150**, 23.

Goldstein, M. E. & Hultgren, L. S. 1988 Nonlinear spatial evolution of an externally excited instability wave in a free shear layer. *J. Fluid Mech.* **197**, 295.

Goldstein, M. E. & Leib, S. J. 1988 Nonlinear roll-up of externally excited free shear layers. *J. Fluid Mech.* **191**, 481.

Ho, C. M. & Huang, L. S. 1982 Subharmonic and vortex merging in mixing layers. *J. Fluid Mech.* **119**, 443.

Huerre, P. 1980 The nonlinear stability of a free shear layer in the viscous critical layer regime. *Phil. Trans. R. Soc. Lond.* A **293**, 643.

Huerre, P. & Scott, J. F. 1980 Effects of critical layer structure on the nonlinear evolution of waves in free shear layers. *Phil. Trans. R. Soc. Lond.* A **371**, 509.

Hultgren, L. S. 1992 Nonlinear spatial equilibration of an externally excited instability wave in a free shear layer. *J. Fluid Mech.* **236**, 635.

Marasli, B., Champagne, F. H. & Wygnanski, I. 1991 On linear evolution of unstable disturbances in a plane turbulent wake. *Phys. Fluids* A **3**, 665.

Marasli, B., Champagne, F. H. & Wygnanski, I. 1992 Effect of travelling waves on the growth of a plane turbulent wake. *J. Fluid Mech.* **235**, 511.

Monkewitz, P. A. & Huerre, P. 1982 The influence of the velocity ratio on the spatial instability of mixing layers. *Phys. Fluids* **25**, 1137.

Oster, D. & Wygnanski, I. 1982 The forced mixing layer between parallel streams. *J. Fluid Mech.* **123**, 91.

Riley, J. J. & Metcalf, R. W. 1980 Direct numerical simulation of a perturbed turbulent mixing layer. *AIAA Paper* 80-0274123.

Roberts, F. A. 1985 Effects of periodic disturbance on structure and mixing in turbulent shear layers and wakes. Ph.D thesis, Cal. Tech., Pasadena.

Robinson, J. L. 1974 The inviscid nonlinear instability of parallel shear flows. *J. Fluid Mech.* **63**, 723.

Strange, P. J. R. & Crighton, D. G. 1983 Spinning modes on axisymmetric jets. *J. Fluid Mech.* **134**, 231.

Weisbrot, I. & Wygnanski, I. 1988 On coherent structures in a highly excited mixing layer. *J. Fluid Mech.* **195**, 137.